

Photoelectron Spectroscopy of Benzoquinone and Dehydrobenzoquinone Anions

Gustavo E. Davico, Rebecca L. Schwartz, Tanya M. Ramond, and W. Carl Lineberger*

Contribution from JILA, University of Colorado and National Institute of Standards and Technology, and Department of Chemistry and Biochemistry, University of Colorado, Boulder, Colorado 80309-0440

Received February 16, 1999

Abstract: The 364 nm photoelectron spectra of the dehydrobenzoquinone ($\mathbf{1}^{\bullet-}$) and benzoquinone ($\mathbf{2}^-$) anions are reported. For $\mathbf{1}^{\bullet-}$, the unambiguous assignment of the origin peak yields an electron affinity (EA) of 1.859 ± 0.005 eV. Several vibrational modes of $\mathbf{1}$ are also reported. Another minor feature at higher electron binding energy is also observed in the spectrum of $\mathbf{1}^{\bullet-}$. This band does not contain any resolvable peaks and only the vertical detachment energy could be obtained. This is the first time dehydrobenzoquinone, the benzyne analogue of *p*-benzoquinone, is observed and characterized. The photoelectron spectrum of $\mathbf{2}^-$ shows no resolvable structure. The origin peak could not be assigned unequivocally because of the small Franck–Condon factor for the 0–0 transition, but an upper value of 2.18 eV for the EA of $\mathbf{2}$ was obtained. Ab initio calculations are used to help in the interpretation of the spectra and the results are utilized to simulate them.

Introduction

Quinones are aromatic compounds with very particular chemical characteristics.¹ One of the most studied of these features is their redox capabilities that, combined with various protonation states, give rise to a variety of structures including semiquinone, hydroquinone, and their corresponding anions and cations.^{2–6} Due to these characteristics, quinones in general, and in particular *p*-benzoquinone derivatives, play a major role in biological reactions, such as the electron-transfer processes of photosynthesis and respiration, and have been detected in a large number of enzymes and proteins involved in these processes.^{7–12} Although the reduced and protonated states of *p*-benzoquinone are relatively well characterized, the deprotonation or dehydrogenation products are completely unknown.

In the gas phase, the information available on these species is even more limited. Only the electron affinity (EA) of *p*-benzoquinone (1.91 eV)^{5,13,14} and an estimate of the EA of

the *p*-benzoquinone radical (2.0 eV)¹⁵ are known. To our knowledge, there is no measurement of the acidity of *p*-benzoquinone, and dehydrobenzoquinone has not previously been obtained or characterized.

In this paper we report the photoelectron spectra of dehydrobenzoquinone anion ($\mathbf{1}^{\bullet-}$) and benzoquinone anion ($\mathbf{2}^-$). Photoelectron detachment of $\mathbf{1}^{\bullet-}$ to form the singlet ground electronic states of $\mathbf{1}$ has been observed and the electron affinity of $\mathbf{1}$ determined. There is vibronic structure in this band, from which vibrational frequencies have been derived. Another low-intensity band at higher electron binding energy is also observed in the spectrum. It shows no vibrational structure and there is no unequivocal assignment for this band. In the case of $\mathbf{2}^-$, the spectrum shows unresolved vibronic structure, and an upper value for the EA of $\mathbf{2}$ has been obtained. To help in the interpretation of the photoelectron spectra of such large and relatively unknown molecules, we performed ab initio calculations on these systems. These theoretical results are also presented in this work as well as simulations of the photoelectron spectra.

Experimental Section

The photoelectron spectrometer and the general experimental procedures have been described previously in detail^{16,17} and only a brief summary is provided here. The apparatus consists basically of four major parts: ion synthesis, mass selection, photodetachment, and electron energy analyzer.

Ions are prepared in a flowing afterglow source at ca. 0.5 Torr of helium buffer gas. The primary $\text{O}^{\bullet-}$ ion is generated by a microwave discharge by seeding the buffer gas with oxygen. This ion can react with hydrocarbons by abstracting both a hydrogen atom and a proton. In the case of quinone, three different isomers could, in principle, arise from H_2^+ abstraction. Nevertheless, it has been shown that in aromatic

(1) Morrison, R. T.; Boyd, R. T. *Organic Chemistry*, 3rd ed.; Allyn and Bacon: Boston, 1980.

(2) Nonella, M. J. *J. Phys. Chem.* **1997**, *101*, 1235.

(3) Raymond, K. S.; Grafton, A. K.; Wheeler, R. A. *J. Phys. Chem. B* **1997**, *101*, 623–631.

(4) Boesch, S. E.; Wheeler, R. A. *J. Phys. Chem.* **1995**, *99*, 8125–8134.

(5) Boesch, S. E.; Grafton, A. K.; Wheeler, R. A. *J. Phys. Chem.* **1996**, *100*, 10083–10087.

(6) Dryhurst, G.; Kadish, K. M.; Schneller, F.; Renneberg, R. *Biological Electrochemistry*; Academic Press: New York, 1982.

(7) Wise, K. E.; Grafton, A. K.; Wheeler, R. A. *J. Phys. Chem. A* **1997**, *101*, 1160–1165.

(8) Eriksson, L. A.; Himo, F.; Siegbahn, P. E. M.; Babcock, G. T. *J. Phys. Chem.* **1997**, *101*, 9496.

(9) Bolton, J. R.; Mataga, N.; McLendon, G. *Electron Transfer in Inorganic, Organic, and Biological Systems*; American Chemical Society: Washington, DC, 1991; Vol. 228, Chapter 10.

(10) Trumpower, B. L. *Function of Quinones in Energy Conserving Systems*; Academic Press: New York, 1982.

(11) Morton, R. A. *Biochemistry of Quinones*; Academic Press: London, 1965.

(12) Thomson, R. H. *Naturally Occurring Quinones III. Recent Advances*; Chapman and Hall: London, 1987.

(13) Kebarle, P.; Chowdhury, S. *Chem. Rev.* **1987**, *87*, 513–534.

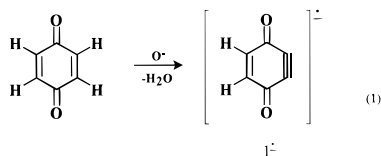
(14) Heinis, T.; Chowdhury, S.; Scott, S. L.; Kebarle, P. *J. Am. Chem. Soc.* **1988**, *110*, 400–407.

(15) Farragher, A. L.; Page, F. M. *Trans. Faraday Soc.* **1966**, *62*, 3072.

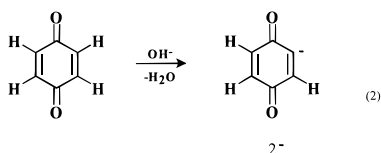
(16) Leopold, D. G.; Murray, K. K.; Stevens-Miller, A. E.; Lineberger, W. C. *J. Chem. Phys.* **1985**, *83*, 4849.

(17) Ervin, K. M.; Lineberger, W. C. *Photoelectron Spectroscopy of Negative Ions*; Adams, N. G., Babcock, L. M., Eds.; JAI Press: Greenwich, 1992; Vol. 1, p 121.

rings the 1,2 abstraction of H_2^+ is the only product observed.^{18,19} Thus, dehydrobenzoquinone anion ($\mathbf{1}^{\bullet-}$) was synthesized by reaction of $\text{O}^{\bullet-}$ with quinone, added downstream in the flow tube according to the reaction shown in eq 1. Benzoquinonide anion ($\mathbf{2}^-$) was prepared by



proton transfer between quinone and OH^- (eq 2), while the latter was synthesized by the well-known reaction of $\text{O}^{\bullet-}$ with methane. Ions



prepared in the flowing afterglow are thermalized at room temperature by collisions with the buffer gas. Liquid nitrogen can be passed through a stainless steel jacket around the flowing afterglow tube to cool the ions below room temperature. The ions formed under these conditions have temperatures around 180–200 K, thus minimizing the presence of hot bands in the photoelectron spectra.

Ions are then extracted from the flowing afterglow tube through a 1 mm orifice in a nosecone into a differentially pumped region where they are accelerated to 735 eV, focused, and mass selected with a Wien filter ($M/\Delta M \approx 40$). This mass resolution is not sufficient to resolve $\mathbf{2}^-$ and $\mathbf{1}^{\bullet-}$; however, a clean spectra of $\mathbf{1}^{\bullet-}$ with negligible contribution from $\mathbf{2}^-$ was obtained by using a low flow of quinone. The $\mathbf{2}^-$ cold spectrum shows some contamination of $\mathbf{1}^{\bullet-}$ even when using very high flows of methane to deplete all the $\text{O}^{\bullet-}$ before it has the chance to react with the quinone, which was added further downstream in the flow tube.

After mass selection, the ions are decelerated to 40 eV prior to entering the laser interaction region. The ion beam is crossed with the 364 nm output of an argon ion laser in a buildup cavity with approximately 100 W of circulating power, as described previously.¹⁷ Photodetached electrons are energy analyzed with a resolution of about 8 meV by using a hemispherical energy analyzer and detected by a position-sensitive detector. Thus, the photoelectron spectra show the number of electrons detected as a function of the electron binding energy, determined by the difference between the laser photon energy (3.408 eV) and the electron kinetic energy.

The absolute energy scale is calibrated by the position of the $^3\text{P}_2 \rightarrow ^2\text{P}_{3/2}$ transition in the $\text{O}^{\bullet-}$ spectrum.²⁰ A small energy compression factor (<1%) is also applied. This factor is determined by the comparison of the peak positions in the spectra of the tungsten ion (W^-) with the known transitions in the tungsten atom.²¹

Molecular orbital calculations were performed with the Gaussian 94 suite of programs.²² Structures were fully optimized at the (U)-B3LYP/aug-cc-pVDZ level^{23–26} by using the standard gradient geometry

(18) Wenthold, P. G.; Squires, R. R.; Lineberger, W. C. *J. Am. Chem. Soc.* **1998**, *120*, 5279.

(19) Leopold, D. G.; Stevens-Miller, A. E.; Lineberger, W. C. *J. Am. Chem. Soc.* **1986**, *108*, 1379.

(20) Neumark, D. M.; Lykke, K. R.; Andersen, T.; Lineberger, W. C. *Phys. Rev. A* **1985**, *32*, 1890–1892.

(21) Moore, C. E. *Atomic Energy Levels*; US GPO Circular No. 467: Washington, 1952.

(22) Frisch, M. J.; Trucks, G. W.; Schlegel, H. B.; Gill, P. M. W.; Johnson, B. G.; Robb, M. A.; Cheeseman, J. R.; Keith, T.; Petersson, G. A.; Montgomery, J. A.; Raghavachari, K.; Al-Laham, M. A.; Zakrewski, V. G.; Ortiz, J. V.; Foresman, J. B.; Cioslowski, J.; Stefanov, B. B.; Nanayakkara, A.; Challacombe, M.; Peng, C. Y.; Ayala, P. Y.; Chen, W.; Wong, M. W.; Andres, J. L.; Replogle, E. S.; Gomperts, R.; Martin, R. L.; Fox, D. J.; Binkley, J. S.; Defrees, D. J.; Baker, J.; Stewart, J. J. P.; Head-Gordon, M.; Gonzalez, C.; Pople, J. A. *Gaussian 94*, Revision E.1; Gaussian, Inc.: Pittsburgh, PA, 1994.

(23) Becke, A. D. *J. Chem. Phys.* **1993**, *98*, 5648.

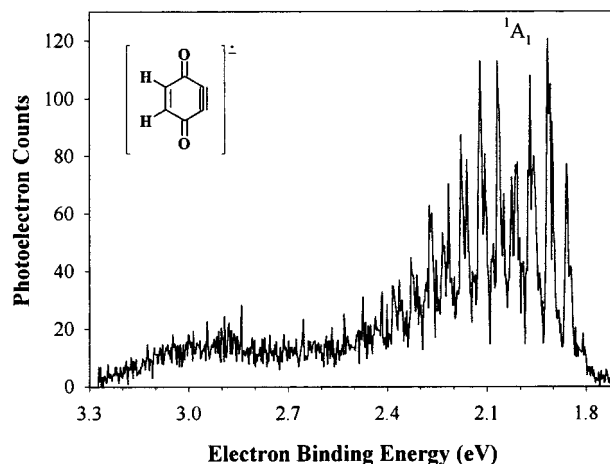


Figure 1. Photoelectron spectrum of dehydrobenzoquinone anion ($\mathbf{1}^{\bullet-}$) at 180 K.

optimization method; the only constraint was maintaining the symmetries specified. Vibrational frequency calculations at the (U)B3LYP/aug-cc-pVDZ level were used to characterize all stationary points as true minima (no imaginary frequencies) and to calculate the zero-point energies (not scaled). Calculations of the Franck–Condon factors were carried out by using a slightly modified version of the program CDECK.²⁷

All reagents were purchased from commercial suppliers and were used without further purification. Quinone 98% was obtained from Aldrich, and other gases were He (99.995%), O_2 (99%), and CH_4 (99.0%).

Results and Discussion

Dehydrobenzoquinone Anion. The photoelectron spectrum of $\mathbf{1}^{\bullet-}$ prepared in a liquid nitrogen cooled flowing afterglow is shown in Figure 1. Two distinct features are observed in the spectrum of this anion, corresponding to the formation of the singlet state of $\mathbf{1}$ (at lower energy) and a low-intensity band (at higher energy) that can be attributed to either a triplet state of $\mathbf{1}$ or a contamination of another anion with the same m/z ratio as $\mathbf{1}^{\bullet-}$, as discussed below.

An expanded view of the lower energy state region is shown in Figure 2. Data obtained at room temperature are shown in Figure 2a while the liquid nitrogen cooled spectrum is shown in Figure 2b. The differences between these spectra clearly show the peaks attributable to hot bands; their intensities are increased drastically at room temperature with respect to the cold data. These hot bands have been labeled with small letters (a–e) and those involving high frequencies in the anion appear only in the room-temperature spectrum, as would be expected. Table 1 lists the frequencies for these transitions as well as their assignments determined with the aid of the calculated values for the low-frequency modes of $\mathbf{1}^{\bullet-}$, shown in Table 2. On the basis of the spectral changes with temperature, the origin of the singlet state (peak A) is determined without ambiguity and has been located at an electron binding energy of 1.859 ± 0.005 eV, the electron affinity of dehydrobenzoquinone. The relative intensity of this peak with respect to the others suggests that the geometry changes moderately in going from the anion to the neutral. The calculations support this conclusion, and optimized geometries corresponding to the C_{2v} point group have

(24) Dunning, T. H. *J. Chem. Phys.* **1989**, *90*, 1007.

(25) Kendall, R. A.; Dunning, T. H.; Harrison, R. J. *J. Chem. Phys.* **1992**, *96*, 6796.

(26) Woon, D. E.; Dunning, T. H. *J. Chem. Phys.* **1993**, *98*, 1358.

(27) We thank Peter Chen and Cameron Logan for providing us with a copy of their CDECK program.

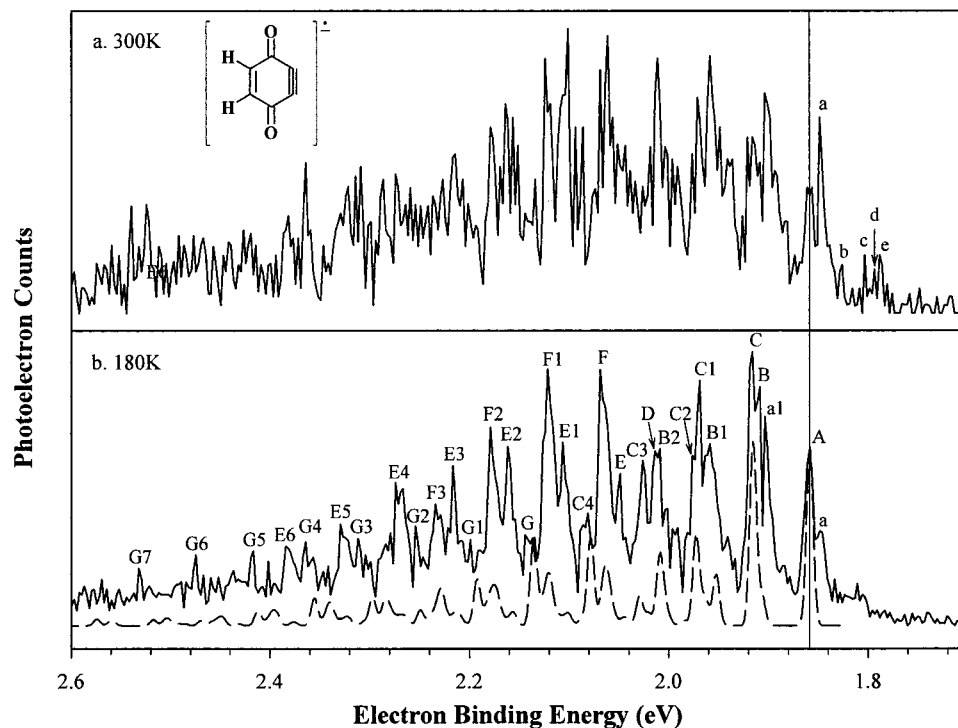


Figure 2. Expanded views of the singlet state region of the photoelectron spectra of dehydrobenzoquinone anion ($1^{\bullet-}$) at room temperature (a) and cooled (b). Assignments of the labeled peaks are provided in Table 1.

Table 1. Peak Positions for Fundamental Frequencies and Assignments for the Photoelectron Spectra of $1^{\bullet-}$

fundamental peak	distance from origin, cm^{-1}	assignment	related peak	assignment
a	80 ± 15	$6_1^1 4_0^1$	a1	$6_1^1 4_0^1 6_0^1$
b	260 ± 20	$3_1^1 0$		
c	460 ± 20	$6_1^1 0$		
d	530 ± 20	$3_2^1 0$		
e	580 ± 20	?		
A	0	0_0^0		
B	405 ± 15	4_0^1	B1	4_0^2
			B2	4_0^3
C	465 ± 15	6_0^1	C1	$6_0^1 4_0^1$
			C2	6_0^2
			C3	6_0^3
			C4	6_0^4
D	1240 ± 20	17_0^1		
E	1535 ± 15	19_0^1	E1	$19_0^1 6_0^1$
			E2	$19_0^1 6_0^2$
			E3	$19_0^1 6_0^3$
			E4	$19_0^1 6_0^4$
			E5	$19_0^1 6_0^5$
			E6	$19_0^1 6_0^6$
F	1685 ± 15	21_0^1	F1	$21_0^1 6_0^1$
			F2	$21_0^1 6_0^2$
			F3	$21_0^1 6_0^3$
G	2285 ± 20	22_0^1	G1	$22_0^1 6_0^1$
			G2	$22_0^1 6_0^2$
			G3	$22_0^1 6_0^3$
			G4	$22_0^1 6_0^4$
			G5	$22_0^1 6_0^5$
			G6	$22_0^1 6_0^6$
			G7	$22_0^1 6_0^7$

been found for both the anion and the neutral. Nevertheless, the calculated EA for **1** does not agree well with the experimental value (Table 3). This result is not surprising as the difficulty of using theoretical methods to calculate accurate differences in energies between species with different numbers of electrons is well-known. Nevertheless, we include the calculated EAs, in part because Schaefer et al. has recently proposed that the same method and a very similar basis set yields EAs with error bars of approximately 0.1 eV on closely related systems.²⁸

Table 2. Frequencies (not scaled in wavenumbers) Determined by (U)B3LYP/AUG-cc-pVDZ Calculations^a

ν	1 (1A_1)	$1^{\bullet-}$ (2A_2)	2 ($^2A'$)	2^-
1	91 (B_1)	122 (B_1)	86 (A'')	98
2	151 (A_2)	279 (A_2)	224 (A'')	247
3	357 (A_2)	378 (A_1)	338 (A'')	300
4	387 (A_1)*	403 (B_2)	400 (A')	393
5	409 (B_2)	407 (A_2)	437 (A')	438
6	461 (A_1)*	476 (A_1)	454 (A')	506
7	559 (B_2)	556 (B_2)	543 (A'')	535
8	605 (B_1)	611 (B_1)	596 (A')	573
9	700 (B_2)	637 (A_2)	742 (A'')	710
10	728 (A_2)	736 (B_2)	752 (A')	767
11	759 (A_1)	770 (B_1)	767 (A')	801
12	851 (B_2)	798 (A_1)	817 (A'')	820
13	858 (B_1)	897 (A_2)	906 (A'')	858
14	979 (A_2)	903 (B_2)	907 (A')	917
15	1021 (A_1)	992 (A_1)	1011 (A'')	985
16	1056 (B_2)	1131 (B_2)	1067 (A')	1080
17	1195 (A_1)*	1152 (A_1)	1165 (A')	1167
18	1309 (B_2)	1322 (B_2)	1221 (A')	1240
19	1633 (A_1)*	1483 (A_1)	1273 (A')	1305
20	1758 (B_2)	1535 (B_2)	1357 (A')	1352
21	1772 (A_1)*	1593 (A_1)	1646 (A')	1520
22	2119 (A_1)*	2020 (A_1)	1680 (A')	1597
23	3190 (B_2)	3141 (B_2)	1710 (A')	1617
24	3208 (A_1)	3162 (A_1)	1726 (A')	1655
25			3178 (A')	3060
26			3180 (A')	3108
27			3201 (A')	3154

^a A_1 modes in **1** are bold and those observed in this work are marked with asterisks.

It is clear from Figure 2 that the peaks labeled with capital letters (B–G) correspond to vibrationally excited transitions within the singlet ground electronic state. This rather complex vibrational structure involves transitions to different quanta of a single frequency as well as several combination bands. The fundamental frequencies associated with these transitions are tabulated in Table 1 along with assignments of all major peaks in the spectrum.

(28) Rienstra-Kiracofe, J. C.; Graham, D. E.; Schaefer, H. F. *Mol. Phys.* **1998**, *94*, 767–787.

Table 3. Adiabatic Electron Affinities (EA), Vertical Detachment Energies (VDE), and Singlet–Triplet Energy Splitting (ΔE_{S-T})^a

	dehydrobenzoquinone (1)		benzoquinonide (2)	
	experiment	theory ^b	experiment	theory ^b
EA	1.859 ± 0.005	2.44 (2.48)	≤2.18	2.18 (2.22)
VDE				
triplet	2.9 ± 0.1			
ΔE_{S-T}	<1.0	1.92 (1.90)		

^a In eV units. The triplet state assignment is tentative (see text for details). ^b Using (U)B3LYP/AUG-cc-pVDZ. The harmonic zero-point vibrational energy corrected values are listed in parentheses.

As seen in Table 1, there are six active frequencies of **1** (B–G) and several related peaks that involve overtones and combination bands. The B progression of peaks (B, B1, and B2) has been assigned to excitations of 1, 2, and 3 quanta of the mode with $\nu_4 = 405 \text{ cm}^{-1}$, respectively. This measured frequency compares very well with the 387 cm^{-1} calculated value for the lowest totally symmetric (A_1) mode of **1** (Table 2). According to the calculations, this normal mode involves the symmetric in-plane bending of the C–O bonds. The calculated value for this mode is only 9 cm^{-1} less in **1**^{•−} than in the neutral, and both compare very well with the 407 cm^{-1} mode found for benzoquinone²⁹ in argon matrices; this indicates that this frequency is not affected by the rather drastic changes between these species. However, according to the extended Franck–Condon progression observed in the spectrum there must be a moderate change in the geometry upon detachment that agrees with the results of the calculations and therefore with the simulated spectra (vide infra).

The progression of peaks labeled C involves excitations of a mode with $\nu_6 = 465 \text{ cm}^{-1}$ to states with 1 (peak C), 2 (peak C2), 3 (peak C3), and 4 (peak C4) vibrational quanta; its value is in excellent agreement with the second A_1 mode calculated for **1**, 461 cm^{-1} (Table 2). This corresponds to a ring deformation mode similar to the $\nu = 600 \text{ cm}^{-1}$ found in the photoelectron spectra of *o*-benzynes.^{18,19} A relatively intense transition (peak C1) is observed and has been assigned to the combination band of modes 4 and 6 both with $\nu = 1$.

The weak transition at 1240 cm^{-1} (ν_{17} , peak D) most likely corresponds to the calculated 1195 cm^{-1} symmetric mode in **1**. This mode consists of the symmetric bending of the C–H bonds. The relatively low intensity and the absence of an observable transition to $\nu = 2$ indicate that the geometries of the neutral and the anion along this normal mode are similar. This is corroborated by comparing the optimized structures obtained from the ab initio calculations that predict a change of only 1 deg for the C(O)–C–H bond angles between the anion and the singlet neutral.

Peak E involves a transition of 1535 cm^{-1} (ν_{19}), which compares well with a value of 1633 cm^{-1} obtained theoretically. These calculations also indicate that the associated normal mode corresponds to the C(H)–C(H) stretching motion. Its activity in the photoelectron spectra correlates with a change of 0.04 \AA in this bond length observed upon detachment in our ab initio calculations. The E₁–E₆ series of peaks has been assigned to combination bands corresponding to excitation of one quantum of ν_{19} with several ($\nu = 1$ –6) excited states of the ν_6 (465 cm^{-1}) mode. Similarly, the F progression of peaks (F1–F3) has been assigned to combination bands involving excitations to $\nu = 1$ –3 of the ν_6 mode with excitation to $\nu = 1$ of the ν_{21} mode (1685 cm^{-1}). The frequency value of this mode (from peak F) agrees

well with the unscaled 1772 cm^{-1} value obtained theoretically. These calculations also show that the normal mode corresponds to the symmetric stretching of the C–O bonds. These C–O bonds are among those that change the most in going from the anion to the neutral; the bond lengths decrease by about 0.05 \AA , which is consistent with the relatively high intensity of peak F with respect to peak A.

A similar picture is observed for peak G and the progression G1–G7. The peak G mode with $\nu_{22} = 2285 \text{ cm}^{-1}$ has been assigned to the C≡C stretching mode, similar to the 1860 cm^{-1} mode observed in the *o*-benzynes^{18,19} photoelectron spectrum; the frequency difference indicates that dehydrobenzoquinone has a stronger triple bond character than the *o*-benzynes. This mode corresponds to the A_1 mode of 2119 cm^{-1} in our ab initio calculation (Table 2). It is interesting to note that our calculations also predict a difference of only 0.01 \AA in the length of the carbon–carbon triple bond between **1** and **1**^{•−}, in agreement with the relatively low intensity peaks displayed in the spectra for these transitions. These findings are in contrast to results obtained for *o*-benzynes,^{30,31} where the change in the carbon–carbon triple bond length upon detachment is about 1 order of magnitude larger than in **1**, and the normal mode associated with the triple bond stretch is the second most active in the spectrum.^{18,19} These results suggest that, in opposition to *o*-benzynes, the detached electron in dehydrobenzoquinone originated from a different orbital than the triple bond π^* orbital, as will be discussed later.

The calculations predict another three totally symmetric modes (A_1) that are not observed in the spectrum or are small enough to be obscured by other transitions. This can be due to the similarity between the anion and the neutral geometries along these normal modes. Analysis of these normal modes shows that this is the case for the 1021 and 3208 cm^{-1} modes, but that the breathing mode with $\nu_{11} = 759 \text{ cm}^{-1}$ should be qualitatively active according to the calculated geometry changes. This mode also has been observed to be active in the photoelectron spectrum of *o*-benzynes.^{18,19} Simulations based on these calculations also suggest that this mode should be active and will be discussed later.

The broad low-intensity feature at higher energy (see Figure 1) does not contain resolvable peaks. The maximum of this band is the vertical detachment energy (VDE), the energy required to form the neutral at the anion geometry. The VDE for this state is at an electron binding energy of $2.9 \pm 0.1 \text{ eV}$, yielding an upper limit for the adiabatic transition. Initially, we assigned this band to the 3B_2 state of **1**. If this were true, the singlet–triplet splitting of **1** is surely less than 1 eV. Our ab initio calculations estimate it to be 1.9 eV (either excluding or including zero-point energy, see Table 3). Further higher level calculations were beyond the scope of the present work. However, during the review process, our results motivated extensive high-level theoretical work by Cramer.³² His high-level theoretical results agree with our calculated singlet–triplet splitting, indicating that the 3B_2 state lies about 1.9–2.0 eV above the 1A_1 state, and therefore should not be detected with our 3.408 eV photon energy. Since angular distribution measurements can give an experimental determination of the orbital from which the electron is detached, we will discuss this issue in more detail after presenting the polarization data.

Angular Distribution Measurements. All the spectra presented in Figures 1 and 2 were taken at the “magic angle” (54.7°)

(30) Nash, J. J.; Squires, R. R. *J. Am. Chem. Soc.* **1996**, *118*, 11872.

(31) Cramer, C. J.; Nash, J. J.; Squires, R. R. *Chem. Phys. Lett.* **1997**, *227*, 311.

(32) Cramer, C. J. Preprint.

(29) McCarthy, W.; Plokhotnichenko, A. M.; Radchenko, E. D.; Smets, J.; Smith, D. M. A.; Stepanian, S. G.; Adamowicz, L. *J. Phys. Chem. A* **1997**, *101*, 7208–7216.

between the laser polarization plane and the photoelectron collection axis. Spectra of $\mathbf{1}^{\bullet-}$ were also taken at the parallel (0°) and perpendicular (90°) polarizations (not shown) by rotating a half-wave plate in the laser path. Equation 3 allows us to estimate the asymmetry parameter^{33,34} β for photodetached electrons:

$$\beta = \frac{I_0 - I_{90}}{(1/2)I_0 + I_{90}} \quad (3)$$

where, for a given peak, I_0 is the intensity in the parallel photoelectron spectra and I_{90} is the intensity for the perpendicular detachment.

The asymmetry parameter provides information about the symmetry of the orbitals from which the electrons are detached. In the case of photodetachment from atoms, since the selection rule is $\Delta l = \pm 1$, electrons coming from s orbitals show p wave detachment ($\beta = 2$), while electrons detached from p orbitals show s wave ($\beta = 0$) or d wave ($\beta = -1$) behavior. The value of β for p orbitals is also a function of the electron kinetic energy, depending on the relative distribution of the s and d waves.

Photodetachment from molecular anions is more complicated, but in general, work in our laboratory has shown that β becomes positive for detachment from σ orbitals and negative or zero for detachment from π orbitals, in the energy range reported in this paper. The important issue is that the photoelectron angular distribution provides a signature of the orbital from which the electron is detached.

Molecular orbital calculations aid in better understanding the processes that are involved in the detachment from $\mathbf{1}^{\bullet-}$ to form the singlet and triplet electronic configurations of $\mathbf{1}$. The molecular orbital diagram for these species is shown in Figure 3. The same scheme has also been plotted for *o*-benzynes for comparison. In the latter, only the two highest occupied molecular orbitals are involved in the detachment process.^{19,30} These orbitals are the bonding (a_1) and antibonding (b_2) carbon-carbon triple bond, respectively, that can be obtained by the symmetric and antisymmetric combination of the lone-pair-like orbitals of the dehydrocarbon atoms.³⁵ As has been shown before and depicted in Figure 3, detachment from the SOMO (b_2) produces the singlet (1A_1) electronic state while detaching one of the electrons from the a_1 orbital gives the triplet (3B_2) state.¹⁹ Both of these states are observed in the photoelectron spectrum of *o*-benzynes.^{18,19} In dehydrobenzoquinone, the perturbation introduced by the carbonyl groups is large enough to change the molecular orbital picture dramatically. As seen in Figure 3, the extra electron in dehydrobenzoquinone goes to a different orbital than in *o*-benzynes. It is clearly a π symmetry orbital (a_2), which lies at lower energy than the b_2 orbital. Detachment from this orbital generates the singlet electronic ground state (1A_1) of dehydrobenzoquinone. The asymmetry parameter for the singlet state obtained from the parallel and perpendicular spectra at the EA peak is -0.52 ± 0.1 , indicating that in this case the electron is detached from an orbital with π symmetry, in perfect agreement with theory. It is interesting to note that the EA of quinone¹⁴ (EA = 1.91 eV) is very similar to that of $\mathbf{1}$ (1.859 eV, Table 3). According to Figure 3, the a_2 orbital (the LUMO in both cases, and therefore, the orbital from which the electron is detached in the anions) is slightly perturbed by

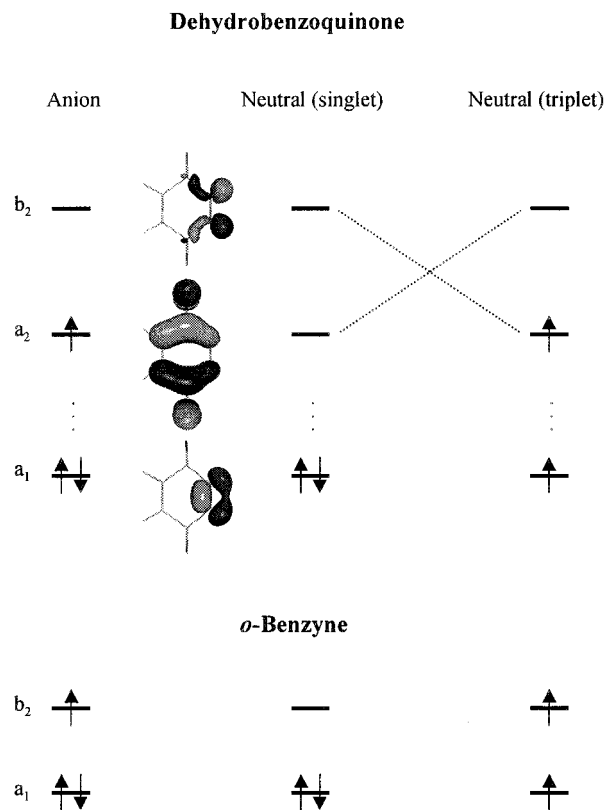


Figure 3. Scheme of the molecular orbital levels for dehydrobenzoquinone anion and singlet and triplet states of the neutral. Energy levels for *o*-benzynes are included for comparison, see ref 35. The molecular orbital plots were obtained from B3LYP/aug-cc-pVDZ wave functions. The a_1 and b_2 orbitals are similar for both dehydrobenzoquinone and *o*-benzynes systems. Note the switch in stability between the a_1 and b_2 orbitals in the triplet state of dehydrobenzoquinone.

the removal of the two hydrogen atoms and the formation of the triple bond.

For the triplet state the process is more complicated than in *o*-benzynes. In this case, the formation of the 3B_2 electronic state in the neutral involves a two-electron process: detachment from the a_1 orbital and promotion of the electron in the a_2 orbital to the b_2 orbital. As seen in Figure 3, detachment from the a_1 orbital produces a rearrangement of molecular orbitals that switch the energy levels between HOMO (a_2) and LUMO (b_2). Therefore, the b_2 orbital becomes more stable than a_2 , resulting in the lowest energy 3B_2 electronic state. The low intensity shown in the photoelectron spectrum for this band is in agreement with this picture. It is interesting that the triplet electronic configuration in dehydrobenzoquinone turns out to be the same as that in *o*-benzynes, even when the initial anion electronic structures are different. The asymmetry parameter determined for this state is 0.1 ± 0.1 , nearly isotropic electron detachment. In principle, this value agrees with the theoretical finding that the electron is detached from a totally symmetric (a_1) molecular orbital, even when the detachment involves a two-electron process. Unfortunately, our DFT calculations not only overestimate the EA of $\mathbf{1}$, but also seem to disagree with higher level ab initio calculations on the configuration of the triplet states. Figure 3 shows the lowest triplet state predicted by B3LYP/aug-cc-pVDZ. Another 3B_2 state lying 0.4 eV above it (at B3LYP/6-31+G* level) has also been found. In this case, the unpaired electrons occupy the a_2 and a b_1 orbital (not shown in Figure 3) that corresponds to the highest occupied π orbital of the aromatic ring. Motivated by the present results, calculations at CAS level (including 10 electrons and 10 orbitals active space³²), predict

(33) Cooper, J.; Zare, R. N. *J. Chem. Phys.* **1968**, *48*, 942.

(34) Cooper, J.; Zare, R. N. *J. Chem. Phys.* **1968**, *49*, 4252.

(35) Wierschke, S. G.; Nash, J. J.; Squires, R. R. *J. Am. Chem. Soc.* **1993**, *115*, 11958.

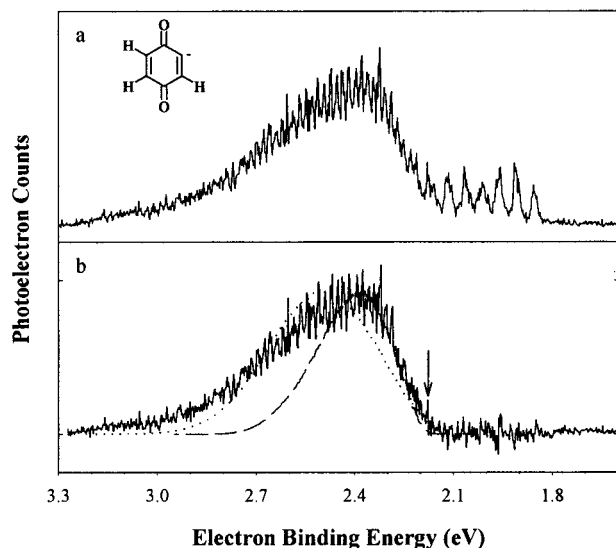


Figure 4. (a) Cold photoelectron spectrum of benzoquinonide anion (2^-). The contamination of $1^{\bullet-}$ appears at lower electron binding energies. (b) Spectrum showed in part a after subtracting the one corresponding to $1^{\bullet-}$ from Figure 1 (solid line); simulated spectrum obtained by using the 16 most active frequencies from the ab initio calculations (dotted line); simulated spectrum obtained by using only the 7 most active frequencies from the calculations (dashed line).

the reverse ordering for these states. If the detachment of one of the electrons of the b_1 orbital to form the latter 3B_2 state (predicted to be the lowest triplet state by Cramer³²) is responsible for the minor feature in the spectrum of $1^{\bullet-}$, we should observe an asymmetry parameter consistent with the detachment of a π electron (as in the case of the singlet), in disagreement with the value of 0.1 observed experimentally. As mentioned above, and based on energetic considerations, Cramer³² suggests that this feature at higher energy in the spectrum of $1^{\bullet-}$ is consistent with the formation of the singlet state of 2,6-dehydroquinone from a contamination of 2,6-dehydroquinone anion that could also be formed in the ion source. Again the asymmetry parameter dissents with this possibility. In agreement with the results of Cramer, calculations on 2,6-dehydroquinone show that the electron is detached from a π orbital, very similar to the a_2 orbital to form the singlet state of **1** (see Figure 3). This indicates that the asymmetry parameter should be the same when forming the singlet states in both isomers, in disagreement with experiment. Thus, at this point, we cannot unambiguously assign this broad structureless feature in the spectrum.

Benzoquinonide Anion. The cold photoelectron spectrum of the benzoquinonide anion (2^-) at the magic angle is plotted in Figure 4a. As can be seen, this spectrum shows some contamination from $1^{\bullet-}$ (see the Experimental Section). The spectrum of $1^{\bullet-}$ slightly overlaps that of 2^- around its origin, obscuring the 0–0 transition and making the determination of the EA for this species more difficult. Removing the contribution from $1^{\bullet-}$, by subtracting the spectrum in Figure 1, gives us the portion generated only by 2^- . The result is shown in Figure 4b. This spectrum does not contain any resolvable progressions of peaks and thus, in contrast to the spectra of $1^{\bullet-}$, no vibrational information can be extracted. Calculations also agree with this picture, suggesting that the geometry goes from C_1 symmetry (no symmetry) in the anion to C_s in the neutral, allowing many degrees of freedom in the neutral to be active. The anion breaks the symmetry in an attempt to distribute the excess charge localized on the carbon atom after the proton is removed. In a planar C_s structure, the charge would be localized on the sp^2

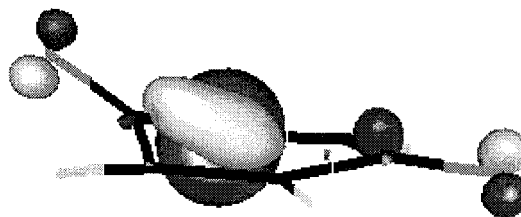


Figure 5. Plot of the highest occupied molecular orbital of 2^- showing the interaction between the back lobe of the nonbonding orbital of the dehydrocarbon with the carbonyl π orbital.

orbital of the dehydrocarbon atom because there is no possibility for this charge to be delocalized in the orthogonal π system. The only chance to donate charge is through the σ bond to the neighboring, highly electron-deficient carbonyl carbon atom. However, if the molecule breaks the C_s symmetry, a direct interaction could be possible between the back lobe of the nonbonding sp^2 orbital and the carbonyl π system. This interaction, in turn, also involves the sacrifice of the aromaticity and the result will depend on which interaction prevails on a purely energetic basis. The latter interaction seems to dominate in this case as the system prefers to bend and move the neighboring carbonyl group out of the plane as shown in Figure 5. In this figure the HOMO of 2^- has also been plotted and clearly shows the kind of interaction described above.

The fact that there are no resolvable peaks in the spectrum also affects the evaluation of the electron affinity. It becomes very difficult to determine where the signal ends and where the noise or hot bands start. Thus, only an upper value for the electron affinity can be obtained by locating the lowest electron binding energy peak that clearly does not originate from $1^{\bullet-}$ contamination, from a residue in the spectra subtraction, or from a hot band by comparing its intensity with the spectrum taken at room temperature (not shown). This peak is identified in Figure 4b with an arrow, and is located at an electron binding energy of 2.18 eV (Table 3). It is interesting to note that, in this case, the calculated EA is in close agreement with the experimental upper limit value (Table 3).

There are no previous quantitative determinations of the EA of **2**. Farragher et al.¹⁵ used the magnetron technique to estimate the electron affinity of *p*-benzoquinone. In this study, they interpreted the results obtained at low temperatures as a C–H dissociative process occurring in the quinone, giving rise to 2^- , and obtained the electron affinity of **2**, 2.000 ± 0.040 eV, based on several assumptions and estimations. Most important of all is the hypothesis that the ion was indeed 2^- , due to the lack of mass analysis of the technique. The error bar assigned seems to be very small, according to estimations used for some physical properties such as the C–H bond dissociation energy and the adsorption energy of the hydrogen atom on the filament surface. Even though the obtained value agreed with that of other substituted phenyl radicals “it is difficult to see why this process should occur at lower temperatures than that of direct capture, and without further proof the interpretation is conjectural” in the authors own words.¹⁵ While their value for the electron affinity of **2** agrees with our upper limit (Table 3), we think this agreement is fortuitous.

Modeling of the Photoelectron Spectra and Franck–Condon Fitting. The analysis of a photoelectron spectrum requires the recognition of the sequence of transitions that correspond to different quanta of a given vibrational mode. The relative intensities of the peaks depend on the Franck–Condon factors, which are a function of geometry changes in the neutral with respect to the anion in the different normal coordinates.

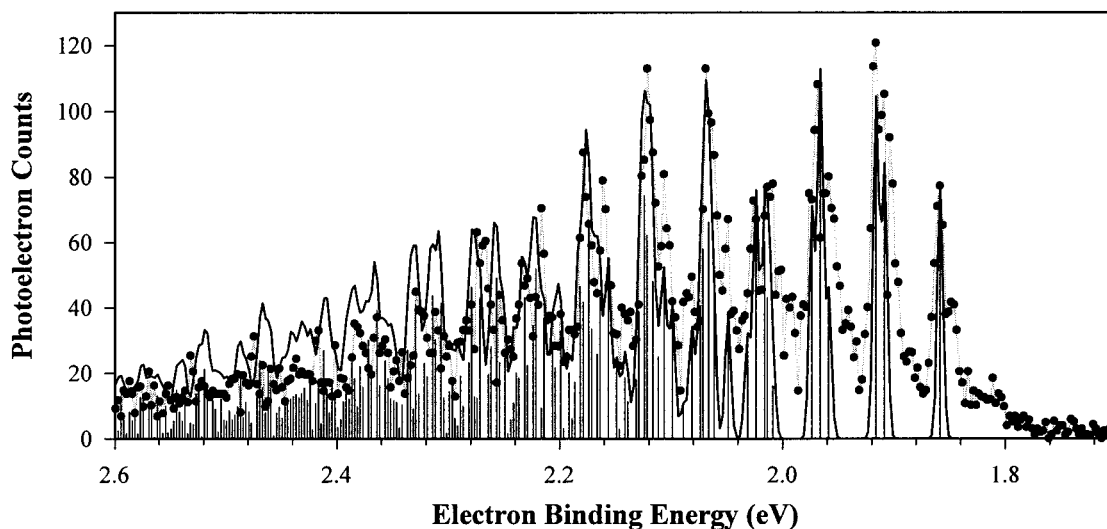


Figure 6. Franck–Condon fit of the photoelectron spectrum of $1^{\bullet-}$. The experimental data are shown as filled circles, individual transitions are shown with sticks, and the convoluted sticks are shown with a solid line.

Thus, the Franck–Condon factors for an electronic transition can be calculated if the geometries, frequencies, and normal modes for the initial and final states are known. Unfortunately, this information is rarely available for ions and radicals. However, it has been shown that estimates of these properties can be obtained from ab initio calculations with sufficient accuracy for modeling photoelectron spectra.³⁶ These parameters are usually much better determined than, for example, relative energies between the anion and neutral states. Chen and co-workers have developed a program suite, CDECK,^{27,36} that calculates the normal modes displacements by reading the frequencies, force constants, and normal modes directly from a GAUSSIAN force constant output file.²² This information is then used to calculate the actual Franck–Condon factors for different transitions by calculating the vibrational wave function overlap between $\nu = 0$ in the anion (and therefore excluding hot bands) and several vibrational states of the neutral. All of these calculations use the harmonic oscillator approximation.

By adjusting the position and height of the origin peak (0–0 transition) and the peak widths by convoluting them with a Gaussian function, the resulting simulated spectrum can be plotted for comparison. Figure 2b shows the simulated and experimental spectra for $1^{\bullet-}$. The simulated spectrum was calculated by using the geometries and frequencies (not scaled) obtained at the B3LYP/aug-cc-pVDZ level of theory and by using a fwhm value of 8 meV. The agreement between the simulated and the experimental spectra is poor compared with results obtained for other anions, even when using lower level calculations. For example, the same method has been used to successfully simulate the photoelectron spectrum of the similar *o*-benzynes anion by using the results obtained at the, rather lower, B3LYP/cc-pVDZ level of theory.¹⁸

The reasons for the poorly simulated spectrum reside mainly in the peak intensities (Franck–Condon factors) but also in the frequency values. Although the observed frequencies are calculated within 4.5% average error, some are calculated almost exactly (like the 461 cm^{-1} mode) while others deviate by as much as 7.3%. For a relatively high-frequency mode such an error will position the simulated transition peak noticeably away from the observed one, as is seen in Figure 2b. The most visible differences between the simulated and the experimental spectra

are the peak intensities. Theory predicts, in principle, that all nine A_1 symmetry modes in the neutral (Table 2) will be active while, as discussed before, only six modes are observed in the spectrum. However, for the $\nu_{15} = 1021$ and $\nu_{24} = 3208$ cm^{-1} modes the intensities are predicted to be too low to be observed. This is in agreement with the fact that these modes are not observed in the spectrum. The other mode not observed experimentally is the 759 cm^{-1} breathing mode; it is observed in the photoelectron spectrum of *o*-benzynes^{18,19} and is predicted to be the third most active mode in **1**. As shown in Figure 3, the origin for the activity of this mode is different for *o*-benzynes than for dehydrobenzoquinone because the electron is detached from different orbitals. For the latter, the increased activity in the simulated spectra for this mode can be rationalized as an overestimation of the bonding properties of the a_2 orbital, causing a bigger contraction of the ring and as a consequence exaggerating the activity of the breathing mode. This difference in activity between the simulated and experimental spectra is accountable for part of the observed discrepancies.

From Figure 2b, it is clear that the most active modes are those associated with peaks C, F, and B (461, 1683, and 404 cm^{-1} , respectively), in agreement with theory that predicts them to be the first, second, and fourth most active modes. Consequently, the main problem in the simulation seems to be not only the relative activities but also the probabilities for overtone transitions, which in the simulation are predicted to vanish more rapidly. These problems could be attributed to a relatively poor estimation of the geometry change between the anion and the neutral, particularly when it is known that very small changes in geometries produce big changes in the peak intensities.

In general, the vibrational intensities in the photoelectron spectrum can also be reproduced by using a Franck–Condon fitting routine described in detail elsewhere.¹⁷ Parameters for the simulation are the vibrational potentials, vibrational frequencies, normal coordinate displacements, temperature, and origin peak position and intensity. The frequency values used are those obtained from the spectrum (Table 1), and the harmonic oscillator approximation was assumed. Since the origin position and intensity were set to match those of the spectrum and a temperature of 300 K was used, the normal coordinate displacements for each of the six normal modes were iteratively optimized to minimize the deviation between the simulated and the experimental spectra. No hot bands were included in the

(36) Chen, P. *Unimolecular and Bimolecular Reaction Dynamics*; Ng, C. Y., Baer, T., Powis, I., Eds.; John Wiley & Sons: New York, 1994.

simulation. Figure 6 depicts the singlet state region of the photoelectron spectrum in symbols; a Franck–Condon analysis of the spectrum is represented with sticks for the position and intensities, and a line is used for the simulation convoluted with a Gaussian peak (fwhm = 8 meV) for each transition. This simulation has been very useful to understand and assign the transitions shown in Table 1. The agreement between the simulation and the spectra is very good considering its complexity. At electron binding energies above 2 eV, each peak consists of multiple transitions that converge after convolution. Only the most important transition is listed in Table 1. The density of transitions shown in Figure 6 gives an idea of the complexity of the spectrum.

Even though the 2^- spectrum does not contain any resolvable peaks, it has been simulated in a similar way as $1^{\bullet-}$ and by using the results from the same theoretical level. In this case, the anion has a geometry corresponding to C_1 symmetry while the radical is C_s (no symmetry). In contrast to normal anions, the ring is bent about 37° from planarity due to the influence of the carbonyl groups as shown in Figure 5 (vide supra). This implies that, in principle, several normal modes of the neutral could be active in the photoelectron spectra. The superposition of all these modes and combination bands contributes to the congested spectrum. Two simulated spectra are plotted in Figure 4b together with the experimental spectrum. The simulation shown with a dotted line includes the first 16 most active modes. The symmetric Gaussian shape of this simulation does not resemble the experimental shape, which is clearly asymmetric. If instead the first seven most active modes are used, the simulation compares better to the experimental results, as can be seen in Figure 4b (dashed line). We interpret these results as an overestimation of the calculations on how far from planarity the anionic structure is predicted to lie, since as it approaches a planar geometry only those modes with a' symmetry will be active while the others will vanish due to symmetry reasons. Nevertheless, both simulations show no

resolved peaks or progression of peaks when using the 8 meV experimental resolution.

Conclusions

We have obtained the photoelectron spectra of dehydrobenzoquinone ($1^{\bullet-}$) and benzoquinonide (2^-) anions. For $1^{\bullet-}$, the unambiguous assignment of the origin peak yields the electron affinity of dehydrobenzoquinone, $EA = 1.859 \pm 0.005$ eV. To our knowledge, this is the first time this structure, which is the benzyne equivalent of 1,4-benzoquinone, is reported in the literature. The spectrum shows rich vibrational structure and it is probably one of the most complex negative ions whose photoelectron spectra contain resolved vibrational structure observed to date. As a result, several fundamental frequencies of **1** could be obtained. Another small feature at higher electron binding energy has been observed in the photoelectron spectrum of $1^{\bullet-}$, but it does not contain any resolvable peaks. The spectrum suggests that there is a significant geometrical change between this state and the anion and thus only the VDE could be obtained, 2.9 ± 0.1 eV. Assignment of this feature is not possible at this point due to disagreement between experiment and theory.

The photoelectron spectrum of 2^- shows no resolvable structure. We conclude that this is a consequence of the many different transitions that are active due to the absence of symmetry in the anion, which generates a high density of peaks. The origin peak could not be assigned, but an upper value of 2.18 eV has been obtained.

Acknowledgment. We specially thank Prof. Christopher J. Cramer for providing his results on the high-level calculations of dehydrobenzoquinone before publication and for stimulating discussion. This work was supported by the National Science Foundation (Grants CHE97-03486 and PHY95-12150).

JA990479Z